Correlation between the characteristic green emissions and specific defects of ZnO

Y. Y. Tay,[ab] T. T. Tan,[a] F. Boey,[b] M. H. Liang,[b] J. Ye,[b] Y. Zhao,[b] T. Norby[c] and S. Li*[a]

Received 26th October 2009, Accepted 16th December 2009
First published as an Advance Article on the web 19th January 2010
DOI: 10.1039/b922372j

In this work, the correlation between the characteristic green emissions and specific defects of ZnO was investigated through a series of experiments that were designed to separate the subtle interplays among the various types of specific defects. With physical analysis and multimode Brownian oscillator modeling, the underlying mechanisms of the variant effects on green emission were revealed. The results demonstrate that the observed green emissions can be identified as two types of individual emissions, namely high energy and low energy, that are associated with specific defects and their locations. The surface modification that leads to downwards band bending was found to be responsible for the high-energy green emission. The relationship between the intensity of the low- energy green emission and the crystallographic lattice contraction indicates that oxygen vacancy is the dominant cause of such an emission that resides within the bulk of ZnO.

1. Introduction

Zinc oxide (ZnO) is perhaps one of the most intriguing materials to be investigated today. Although it has a simple closely-packed hexagonal crystal structure, it possesses many unique properties for various cutting-edge applications, such as sensors and catalysis. Interestingly, ZnO has a diverse range of nanostructural configurations including quantum dots, nanobelts, nanorings, nanosprings, nanobows, nanohelices, nanocages, nanowires, nanospheres and microcheerios. These nanostructural materials are important as building blocks for the architecture of nanodevices.[1–3] In fact, its pre-eminence is also well noted in the field of spintronics and photonics. As a wideband gap semiconductor with a direct bandgap of 3.3 eV at 298 K, it has a brilliant UV band edge emission that can be applied for UV light emitters.[4] However, various synthesis methodologies may influence the appearance of defects which drastically alter UV emission behaviors of ZnO,[5] resulting in new optical phenomena, such as visible emissions of green,[6,7] yellow and red. Among these, the green emission is the most commonly observed phenomenon.[8]

The origin of green emission however has been widely debated. It is believed that deep level defects, such as oxygen vacancies in a form of a singly ionized V_o^+ center or a doubly ionized V_o^{++} center, zinc vacancies and interstices, are possible causes of the green emissions in ZnO.[8] Such emissions have diverse spectra with different peak emission wavelengths from ~510 nm (~2.43 eV)[7] to ~550 nm (~2.25 eV).[9] Spectrometer configurations, such as the power and excitation energy of the laser used in different laboratories are extrinsic factors leading to slight variation of the spectra. Experimental results suggested that the location of point defects, such as surface defects *etc.* has a strong influence on the green emission.[6] The absorption depth of the excitation beam depends on the excitation source as well as the absorption coefficient of ZnO and it has been shown that the penetration depth of a laser (using a 325 nm He–Cd laser) is about 70 nm.[10] In such a shallow depth, it is difficult to discriminate the contribution of the surface defects from the bulk defects on the green emission.

In the present work, we discriminate the surface defects from the bulk defects and investigate their interaction that result in the observed subtle variation of the green emissions. Such a variation can be divided into two particular individual emissions referred to as the high- and low-energy green emissions. This finding may provide some new insights into the fundamental principle of manipulating the emission spectra with defect chemistry for practical applications.

2. Experimental

To separate the subtle changes of the visible emission, the as-received ZnO powder (99.5% pure, Analyticals Carlo Erba) was annealed in a reducing atmosphere of 3% H_2 + 97% Ar from 500 to 900 °C for 24 h. For comparison, the as-received ZnO was also annealed in pure nominally dry N_2, in nominally dry 100% O_2, or in ambient atmosphere which could be considered as a mixture of 21% O_2 + 79% N_2. Photoluminescence (PL) spectra were determined by an Accent Rapid Photoluminescence Mapping System with a He–Cd laser source (325 nm). Here, we denote the defects induced by annealed the ZnO in the reducing atmosphere as 'Type I' defects while those induced in the ambient atmosphere annealing as 'Type II'. A constant power of 1.8 mW was maintained to eliminate the possibility of UV to defect emission intensity ratio variation. The materials were characterized using X-ray

[a] *School of Materials Science and Engineering, The University of New South Wales, NSW 2052, Australia. E-mail: sean.li@unsw.edu.au*
[b] *School of Materials Science and Engineering, Nanyang Technological University, Singapore 639798*
[c] *Department of Chemistry, University of Oslo, SMN, FERMiO, Gaustadalleen 21, NO-0349 Oslo Norway*

diffraction (XRD) with a sampling pitch of 0.02° and scanning rate of 1° min^{-1}. Rietveld analysis was carried out by a Fundamental Parameter procedure as implemented on the TOPAS package to determine the unit cell volume. Furthermore, X-ray photoelectron spectroscopy (XPS) was performed with 20 eV pass energy and the results were subsequently calibrated by the adventitious carbon C 1s peak at 285 eV. The morphologies of the as-prepared materials in powder form were characterized by transmission electron microscopy (TEM).

3. Results and discussion

3.1 PL results and multimode Brownian oscillator model (MBO)

Fig. 1 plots the spectra of the normalized emission intensity *vs.* energies for the materials with Type I and Type II defects induced at 900 °C. The spectrum with Type I defects exhibits a high-energy green emission peaked at 2.465 eV (503.4 nm labelled with "A") while spectrum with Type II defects has a low-energy green emission with peak intensity at 2.294 eV (540.9 nm, labelled with "B"). These differ from the spectra of the as-received ZnO which possess a yellow emission at 2.103 eV (590.0 nm labelled with "C"). The green band which includes the phonon sideband is associated with the interactions between the electronic degrees of freedom and optical phonons. Therefore, it is interesting to simulate the green emission band with the multimode Brownian oscillator (MBO) model and then extract the useful information on electron–phonon coupling of the materials. In the MBO model, the Hamiltonian of the system can be described by:[11]

$$H = |g\rangle H_g\langle g| + |e\rangle H_e\langle e| + H' \quad (1)$$

where

$$H_g = \sum_j \left[\frac{p_j^2}{2m_j} + \frac{1}{2}m_j\omega_j^2 q_j^2\right] \quad (2)$$

$$H_e = \hbar\omega_{eg}^0 + \sum_j \left[\frac{p_j^2}{2m_j} + \frac{1}{2}m_j\omega_j^2 (q_j + d_j)^2\right] \quad (3)$$

and

$$H' = \sum_n \left[\frac{P_n^2}{2m_n} + \frac{1}{2}m_n\omega_n^2\left(Q_n - \sum_j \frac{c_{nj}q_j}{m_n\omega_n^2}\right)^2\right] \quad (4)$$

In eqn (1)–(4), P_j (P_n), q_j (Q_n), m_j (m_n) and ω_j (ω_n) are the momentum, coordinate, mass and angular frequency of the jth (nth) nuclear mode of the primary (bath) oscillators, respectively. In eqn (3), d_j is the displacement of the jth nuclear mode in the electronic excited state. The term $\hbar\omega_{eg}^0$ represents the energy difference in the two-level system. H' can be regarded as the coupling between the primary oscillators and bath modes with a coupling strength of c_{nj}. The key parameters of the MBO model are the frequencies of the primary oscillators ω_j, the damping coefficient γ_j that controls the system–bath coupling strength, and the Huang–Rhys factor S_j which reflects the electron–LO phonon coupling

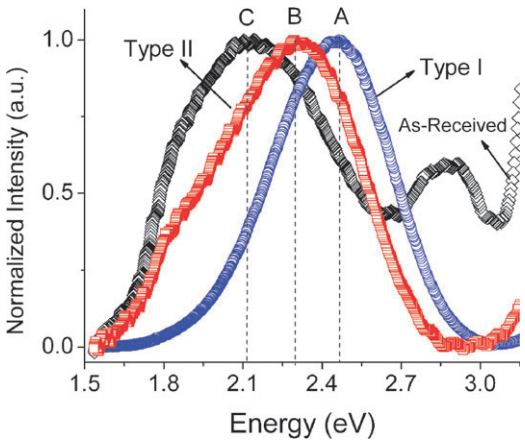

Fig. 1 PL spectra of the as-received ZnO and ZnO with high- and low-energy green emissions with Type I and II defects, respectively, annealed at 900 °C for 24 h.

strength. Other controlling parameters include the bath temperature T and the 0–0 electronic transition energy [or also known as Zero Phonon Line (ZPL), $\hbar\omega_{eg}$].[12] Here we take the LO phonon as the only primary phonon in the model, so $\omega_j = \omega_{LO}$. The LO phonon frequency ω_{LO} is assigned to be the spacing between adjacent phonon side bands. One of the advantages of using MBO is that one could locate the 0–0 electronic transition energy which is difficult to determine by visual inspection.

The spectral density of the MBO model can be written as

$$\tilde{C}''(\omega) = \frac{2\lambda\omega_{LO}^2\omega\gamma(\omega)}{\omega^2\gamma^2(\omega) + [\omega_{LO}^2 + \omega\Gamma(\omega) - \omega^2]^2} \quad (5)$$

where $\Gamma(\omega)$ is the real part of the self-energy and the Stokes shift is given by

$$2\lambda = \frac{m\omega^2 d^2}{\hbar} \quad (6)$$

Alternatively, we can write $\lambda = S\hbar\omega_{LO}$. Here we adopt a simple form of the MBO model in this work. In this model, the spectral distribution function $\gamma(\omega)$ is assumed to be in its Ohmic limit (*i.e.*, $\gamma(\omega)$ = constant). Under these simplifications, the spectral density function has following form

$$C''(\omega) = \frac{2\lambda\omega_{LO}^2\omega\gamma}{\omega^2\gamma^2 + (\omega_{LO}^2 - \omega^2)^2} \quad (7)$$

where the self-energy term $\Gamma(\omega)$ is set to zero.

The spectral response function $g(t)$ can be expressed in terms of the correlation function described in eqn (7) as

$$g(t) = \frac{1}{2\pi}\int_{-\infty}^{\infty} d\omega \frac{C''(\omega)}{\omega^2}[1 + \coth(\beta\hbar\omega/2)][\exp(-i\omega t) + i\omega t - 1] \quad (8)$$

Finally, the PL line shape can be calculated from

$$I_{PL}(\omega) = \frac{1}{\pi}\mathrm{Re}\int_0^{\infty} \exp[i(\omega - \omega_{eg} + \lambda)t - g*(t)]dt \quad (9)$$

whre $g^*(t)$ is the complex conjugate of the line broadening function $g(t)$. Previously, the MBO model was successfully implemented to study the green bands of ZnO.[13] Some of the

parameters used can be implemented as constraints in our work in order to fit our spectra with the MBO model. Firstly, we fix the difference in the two ZPL lines separated by 30 meV as observed in the literature.[13] The two Huang–Rhys factors S_1 and S_2 have a common electron–phonon coupling strength while γ_1 and γ_2 are fixed at 65 and 60 cm^{-1}, respectively, at room temperature. The weight coefficients used to calculate the overall emission spectra are fixed at 1 and 1.5 for $\hbar\omega^0_{e1g}$ and $\hbar\omega^0_{e2g}$. In our earlier studies, we determined our LO phonon frequency to be 583.7 and 582.1 cm^{-1} for the ZnO with Type I and Type II defects, correspondingly.[14] These frequencies are used as the primary oscillator in the MBO model.

Fig. 2 shows the typical measured and calculated emission spectra associated with Type I and II defects while Table 1 shows the fitting results. The PL emissions associated with Type I defects [Fig. 2(a)] can be fitted well with MBO model on the higher energy side. Fig. 2(b) shows the MBO fitting for the PL emissions of ZnO with Type II defects which exhibits a shoulder beside the lower energy green emission. This may be the residual peak from the as-received sample (Fig. 1). This shoulder is believed to be related to the yellow and orange emissions but their origin remains unknown as several types of defects might be responsible for these emissions.[8]

Although the shoulder emission causes the overall fitting to be less satisfactory, the objective of this work is to extract information on the green band, hence MBO fitting is needed on the higher energy side of the low-energy green emission associated with Type II defects. This region allows the MBO fitting to provide valuable information on the 0–0 transition energies (ZPL) as well as the Huang–Rhys factor that are responsible for the green emission [Fig. 2(b)].

From Fig. 3, it can be seen that the 0–0 transition energies for both high- and low-energy green emissions have a slight increase with increasing inducing temperature. On the other hand the electron–phonon coupling strength represented by the Huang–Rhys factor also increases with increasing temperature in the emissions associated with both types of defects. Both the increasing 0–0 transition energy and the Huang–Rhys factor could be attributed to the amount of mean surrounding lattice distortion which increases with defect concentration as a function of temperature.[15,16]

Table 1 Fitted parameters using the MBO model on ZnO annealed in the ambient (Type II) and reducing (Type I) atmospheres at different temperatures

	Conditions	$\hbar\omega^0_{e1g}$	$\hbar\omega^0_{e2g}$	ω_{LO}	$S_1 = S_2$
Type I defects	500 °C, 24 h	2.951	2.981	583.7	7.3
	700 °C, 24 h	2.981	3.011	583.7	8.1
	900 °C, 24 h	3.021	3.051	583.7	8.65
Type II defects	500 °C, 24 h	2.841	2.871	582.1	8.2
	700 °C, 24 h	2.841	2.871	582.1	8.4
	900 °C, 24 h	2.911	2.941	582.1	8.85

Although the 0–0 transition energy of the emission associated with Type I defects is always higher than that with Type II defects [Fig. 3(a)], it does not follow that ZnO would have a higher concentration of Type I defects than that of Type II. This is because the Huang–Rhys factor as observed in high-energy green emission is always lower than that of the low-energy one [Fig. 3(b)]. It implies that the Huang–Rhys factor is dependent on the nature of defects.[12] This observation suggests that the mechanism of high- and low-energy green emissions may be different.

3.2 Influence beneath the surface

Fig. 4(a) shows the increase in the emission intensities with the defect inducing temperature. They could be attributed to the increase of the emission transition site concentration which is directly related to the defect of interest thus indicating that the defect concentration increases with inducing temperature.[17]

On the other hand, Fig. 4(b) shows the unit cell volume determined from Rietveld refinement of the XRD results for the ZnO with Type I and II defects. It is necessary to take note that the unit cell volume contraction is smaller at the inducing temperature of 700 °C for ZnO with Type I defects which would imply a lower defect concentration. This is unexpected as the observed increasing high-energy green emission intensity implies an increasing defect concentration [Fig. 4(b)]. Therefore, the donors/defects that cause the volume contraction may not be the cause responsible for the high-energy green emission associated with Type I. The gradual volume contraction for ZnO with Type II defects indicating a continuous increase in defect concentration is however consistent with its increasing

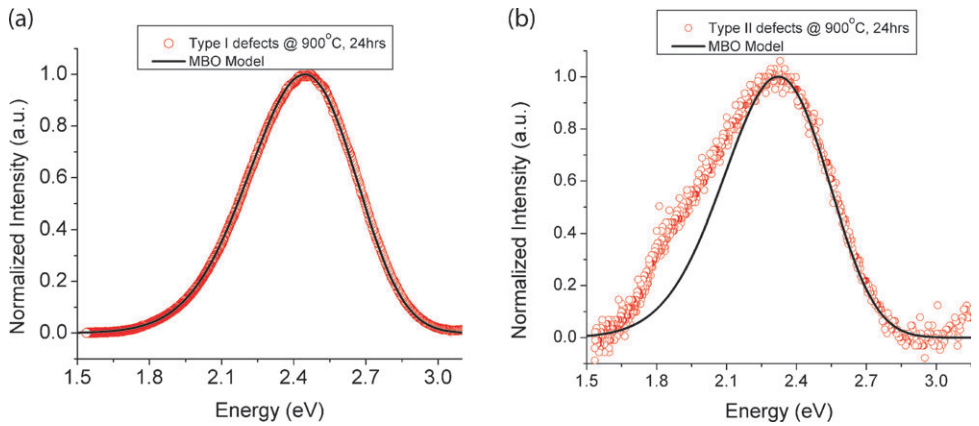

Fig. 2 MBO model fitting of ZnO of (a) Type I and (b) Type II defects annealed at 900 °C respectively.

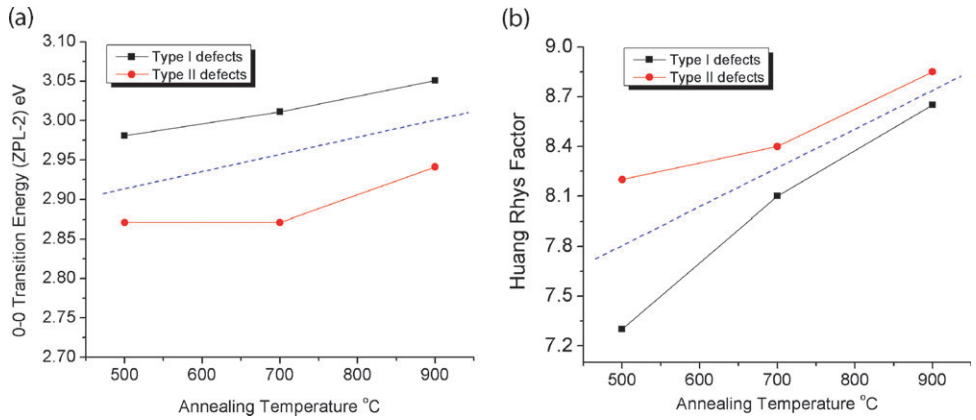

Fig. 3 (a) 0–0 transition energy for ZPL-2 ($\hbar\omega^0_{e2g}$) and (b) Huang–Rhys factor (S) for ZnO of Type I and II defects annealing at different temperatures. Note that only ZPL-2 is shown for simplicity since $\hbar\omega^0_{e1g}$ and $\hbar\omega^0_{e2g}$ are constrained by a difference of 30 meV. The dashed lines in both figures shows a clear difference between the nature of Type I and Type II defects.

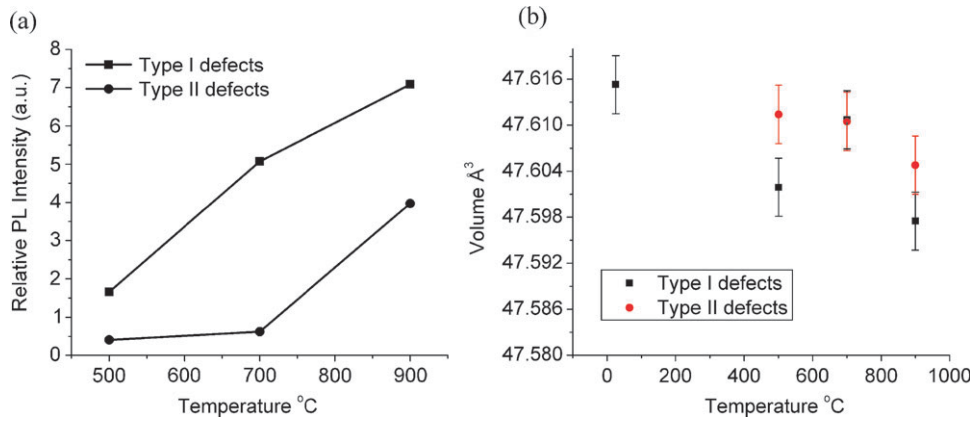

Fig. 4 (a) Relative PL intensity (normalized with reference to UV emission) trend with increasing temperature and (b) XRD Rietveld refinement unit cell volume of ZnO with Type I and II defects as a function of inducing temperature.

lower energy green emission intensity. This indicates that the defects may have been originated from the bulk. It also suggests that the defects are found within the absorption depth of the He–Cd laser ($\sim$70 nm).

For a deeper understanding of the specific defects that influence the PL emissions, we also treated the ZnO in pure oxygen atmosphere. Fig. 5 shows the emission spectra of the ZnO processed in such atmosphere and the low-energy green emission associated with Type II defects with peak emissions at 2.186 (eV) (567.5 nm) and 2.294 eV (540.9 nm), respectively. The difference is clear. Despite that these ZnO samples are annealed with similar zinc partial pressure, it is less likely that they have similar defect origin that relates to their emissions such as zinc vacancies. In fact, by reducing the oxygen partial pressure from 1 atm to 0.21 atm, the emission intensity peaked at 2.186 (eV) becomes weaker while the low-energy green emission associated with Type II defects becomes dominant.

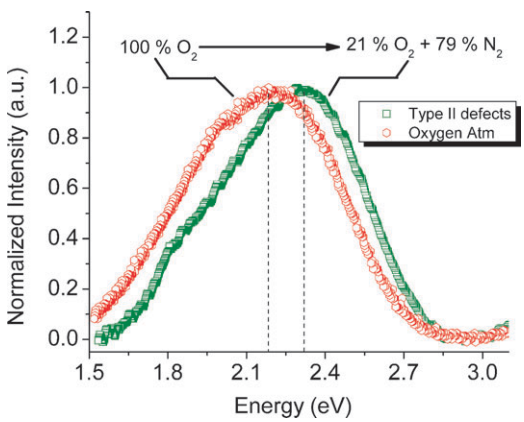

Fig. 5 PL spectra of ZnO with Type II defects annealed at 900 °C for 24 h and under O_2 atmosphere at 900 °C for 24 h.

3.3 Influence from surface modification

To identify the nature of defects and understand how the specific defects give rise to the particular green emissions, the surfaces of the as-prepared materials were characterized with XPS. The as-received ZnO, which serves as the reference, has a core level Zn $2p_{3/2}$ binding energy (BE) at 1021.2 eV. The BE of Zn $2p_{3/2}$ for the ZnO with Type I defects is 1.8 eV higher (1023.0 eV) while the ZnO with Type II defects shifts towards lower energy by 0.5 eV [Fig. 6(a)]. This shows that the core level BE of ZnO with both green emissions shifts in the opposite directions to that of the as-received materials. It is

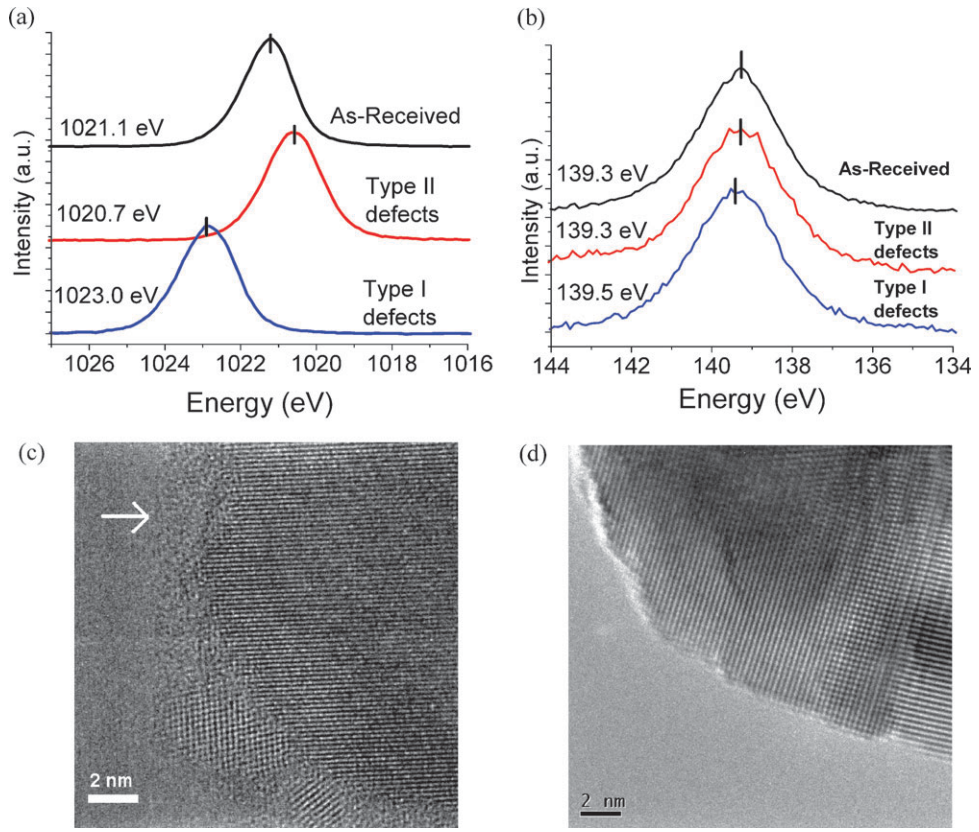

Fig. 6 (a) XPS spectra of Zn $2p_{3/2}$, (b) Zn 3s for the ZnO with Type I and II defects, respectively, annealed at 900 °C for 24 h. High-resolution TEM image of ZnO with (c) Type I defects (annealed at 900 °C, 24 h) with an ultra-thin modified layer (arrowed) and (d) with Type II defects (annealed at 900 °C, 24 h).

interesting to note that the other measured core level orbital BE, Zn 3s has a small distinctive shift of 0.2 eV for ZnO with Type I defects [Fig. 6(b)].

The BE shift that occurs at the Zn $2p_{3/2}$ core level may be associated with the sensitivity of the maximum sampling depth of XPS characterization. The electron inelastic mean free path (IMFP) α (Å) could be estimated at a particular binding energy using the Tanuma–Powell–Penn TPP2M formula.[18] The maximum sampling depth was subsequently derived from the decaying function $\exp(-d/\alpha)$,[19] where d is the approximated sampling depth. Since d is approximated by 3α, in this depth ~95% of all the photoelectrons would be scattered by the time they reach the surface. The calculation shows that the estimated maximum sampling depth for Zn $2p_{3/2}$ is about 3.5 nm while it is approximately 7.6 nm for Zn 3s, respectively. This indicates that a dominant modification may have occurred on the surface of the material processed in the reducing atmosphere and the depth of the modified layer underneath the surface was less than 3.5 nm.

Pertaining to the first observation, as the shift for ZnO with Type I defects is much larger, an extensive modification may have taken place on the surface. Since the core level BE of Zn 3s has shifted only slightly, little modification occurred at the corresponding sampling depths. The XPS results are supported by the high-resolution TEM image in Fig. 6(c) and (d). The high-resolution image in Fig. 6(c) shows that the ZnO with Type I defects has a core shell-like structure with a shell thickness of ~40 Å, in good agreement with the XPS results. Since the shift of the $2p_{3/2}$ core level BE of ZnO with Type II defects is much smaller than that of ZnO with Type I defects, the modification on the surface as shown in the TEM image is not apparent [Fig. 6(d)].

The surface modification in ZnO with Type I defects should be the predominant factor of the high-energy green emission. Such a phenomenon can be explained with the presence of surface band bending. The as-received ZnO has a hydroxylated surface that contributes electrons to form a downwards band bending with an accumulation layer.[20] Since the BE of ZnO with Type I defects shifts to higher energy, there is an increase downwards band bending with the core levels as well as the valence band maximum[21] shifting away from the Fermi level. This could be due to an increased electron accumulation layer possibly from the surface oxygen vacancies which is an electron donor.[22] The ZnO with Type II defects should have a lower degree of downwards band bending as a result of reduced oxygen vacancy concentration.[23] However, such observation should be accompanied by an increase in oxygen vacancy concentration as a function of depth and dominate in the bulk as characterized by XRD and Raman spectroscopy.[14,23] The nature of band bending found in ZnO probably leads to different electronic transitions such as the high- and low-energy green emissions. In addition, it should be noted that the calculated defect transition level of surface oxygen vacancies also appears to be different from the

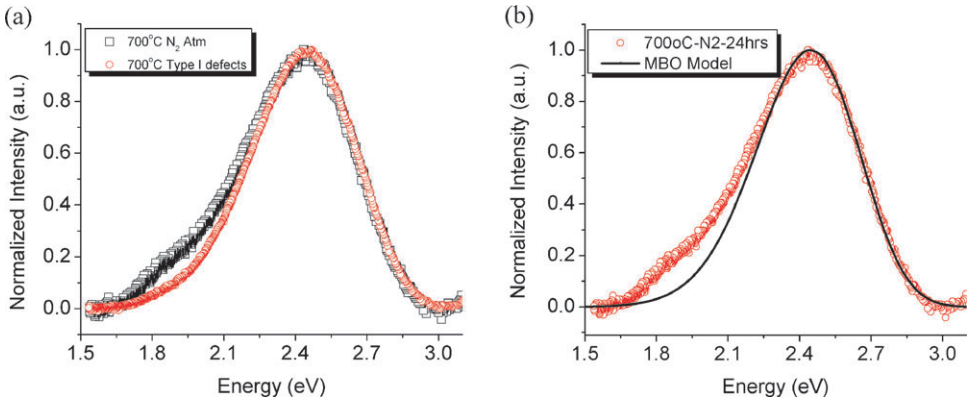

Fig. 7 (a) PL spectra of ZnO with Type I defects and ZnO annealed under nitrogen atmosphere at 700 °C for 24 h and (b) MBO model fitting of ZnO annealed under nitrogen atmosphere at 700 °C for 24 h.

bulk oxygen vacancies leading to these two types of emissions.[24] The higher energy green emission could be due to: (1) a recombination between the oxygen vacancies and the photo-generated holes near the surface,[25] and (2) the modification of the surface that may possess heterostructure of ZnO, thus varying the electronic structure.[26] Detailed investigations will be reported in the future.

3.4 Possibility of hydrogen effects on the green emission

It is unclear whether the hydrogen in a reducing atmosphere would be doped into the materials, thus making a contribution to the high-energy green emission. In general, hydrogen could be a shallow donor dissolved interstitially so that it can be completely ionised to protons, thus residing on oxide ions as hydroxide ion defects and electrons. Such hydrogen easily dominates the defect structure as well as the electrical and photonic properties directly or indirectly. In the reducing atmospheres, hydrogen could be trapped in ZnO above 500 °C, leading to the dissolution of protons and electrons. In the as-reduced materials, the induced defects such as proton and electrons *etc*. would be frozen and trapped in the quenching processing.

The question is: Does hydrogen play a direct role in the development of the high-energy green emission? To isolate the contribution of hydrogen and oxygen on the specific green emissions, we annealed the ZnO in dry N_2 at 700 °C for 24 h. The PL spectra of the materials processed in dry N_2 and 3% H_2 + 97% Ar at 700 °C for 24 h were plotted in Fig. 7(a) for comparison. Fig. 7(b) shows the PL emission spectra of ZnO processed in N_2 at 700 °C with its fitting results using the same MBO parameters obtained from the Type I defects induced at similar temperature. It demonstrates that the MBO fitting is satisfactory at the high-energy band side. Similar emission mechanism appearing in the materials processed in H_2-free atmosphere shows that the high-energy green emission is not originated from hydrogen. In addition, it has been reported that the presence of hydrogen in ZnO enhances the efficiency of UV emission while it suppresses the defect emission, for example, green emission.[27,28] The relative intensity of the high-energy green emission [Fig. 4(b)] was however enhanced in our experiments by the processing temperature. Hence hydrogen seems not to play a direct role in the origination of this green emission.

4. Conclusion

The intrinsic variants of green emissions in ZnO were investigated to separate the subtle interplay among the specific defects. Through systematic experimental separations, advanced materials characterizations and physical modeling, the subtle variation of the green emission was deemed significant and was closely related to the defects residing at different locations. It was found, for example, that the defects residing on the surface and in the bulk give rise to the high-energy (peak value of 2.465 eV) and low-energy green (peak value of 2.294 eV) emissions, respectively. Importantly, the ZnO with Type I defects that are associated with the surface defects, was found to be responsible for the high-energy green emission as evidenced by the downwards band bending through a binding energy shift of Zn $2p_{3/2}$ orbital and the observation of a modified surface layer. The downward band bending caused by the electron accumulation layer could be due to the formation of the surface oxygen vacancies acting as the electron donors. On the other hand, the correlation between the unit cell volume contraction through XRD and PL intensity of the low-energy green emission suggests that the Type II defects are oxygen vacancies distributed beneath the surface. The experimental results also demonstrate that the green emissions are independent of hydrogen doping. This finding provides a new insight that could possibly assist the precise manipulation of the photonic emissions of ZnO for optoelectronic applications in the future.

Acknowledgements

One of the authors (Y. Y. Tay) would like to thank Singapore Millennium Foundation (SMF) for a scholarship. This research is supported by Australian Research Council Discovery Program No. DP0988687. The authors would like to thank Mr K. W. Tye for sample preparation, Dr M. Schreyer and Mr T. Sun for their kind assistance.

References

1 C. Yan and D. Xue, *J. Phys. Chem. B*, 2006, **110**, 1581.
2 Z.-L. Wang, *J. Phys.: Condens. Matter*, 2004, **16**, R829.
3 S. Li, Z. W. Li, Y. Y. Tay, J. Armellin and W. Gao, *Cryst. Growth Des.*, 2008, **8**, 1623–1627.
4 S. Nakamura, M. Senoh, S. Nagahama, N. Iwasa, T. Yamada, T. Matsushita, H. Kiyoku, Y. Sugimoto, T. Kozaki, H. Umemoto, M. Sano and K. Chocho, *Appl. Phys. Lett.*, 1998, **72**, 211.
5 C. Yan and D. Xue, *Electrochem. Commun.*, 2007, **9**, 1247.
6 D. Li, Y. H. Leung, A. B. Djurisic, Z. T. Liu, M. H. Xie, S. L. Shi, S. J. Xu and W. K. Chan, *Appl. Phys. Lett.*, 2004, **85**, 1601.
7 K. Vanheusden, C. H. Seager, W. L. Warren, D. R. Tallant and J. A. Voigt, *Appl. Phys. Lett.*, 1996, **68**, 403.
8 U. Ozgur, Y. I. Alivov, C. Liu, A. Teke, M. A. Reshchikov, S. Dogan, V. Avrutin, S. J. Cho and H. Morkoc, *J. Appl. Phys.*, 2005, **98**, 041301.
9 A. van Dijken, E. A. Meulenkamp, D. Vanmaekelbergh and A. Meijerink, *J. Phys. Chem. B*, 2000, **104**, 1715.
10 J.-i. Takahashi and T. Makino, *J. Appl. Phys.*, 1988, **63**, 87–91.
11 J. Ye, Y. Zhao, N. Ng and J. Cao, *J. Phys. Chem. B*, 2009, **113**, 5897.
12 W. Hayes and A. M. Stoneham, *Defects and Defect Processes in Nonmetallic Solids*, John Wiley & Sons Inc., New York, 1985.
13 S. L. Shi, G. Q. Li, S. J. Xu, Y. Zhao and G. H. Chen, *J. Phys. Chem. B*, 2006, **110**, 10475.
14 Y. Y. Tay, T. T. Tan, M. H. Liang, F. Boey and S. Li, *Appl. Phys. Lett.*, 2008, **93**, 111903.
15 J. Pelzl, *Phys. Status Solidi A*, 1971, **8**, 161.
16 J. Krustok, J. Madasson, K. Hjelt and H. Collan, *J. Mater. Sci.*, 1997, **32**, 1545.
17 L. Pavesi and M. Guzzi, *J. Appl. Phys.*, 1994, **75**, 4779.
18 S. Tanuma, C. J. Powell and D. R. Penn, *Surf. Interface Anal.*, 1994, **21**, 165.
19 D. Briggs and M. P. Seah, *Practical Surface Analysis by Auger and X-ray Photoelectron Spectroscopy*, John Wiley & Sons Ltd., Chichester, 1st edn, 1983.
20 B. J. Coppa, C. C. Fulton, P. J. Hartlieb, R. F. Davis, B. J. Rodriguez, B. J. Shields and R. J. Nemanich, *J. Appl. Phys.*, 2004, **95**, 5856.
21 E. Böhmer, F. Siebke and H. Wagner, *Fresenius' J. Anal. Chem.*, 1997, **358**, 210.
22 W. Göpel and U. Lampe, *Phys. Rev. B: Condens. Matter*, 1980, **22**, 6447.
23 G. D. Mahan, *J. Appl. Phys.*, 1983, **54**, 3825.
24 J. D. Prades, A. Cirera, J. Ramon Morante and A. Cornet, *Thin Solid Films*, 2007, **515**, 8670–8673.
25 Y. Gong, T. Andelman, G. Neumark, S. O'Brien and I. Kuskovsky, *Nanoscale Res. Lett.*, 2007, **2**, 297–302.
26 Q. Lu, Z. Wang, J. Li, P. Wang and X. Ye, *Nanoscale Res. Lett.*, 2009, **4**, 646–654.
27 T. Sekiguchi, N. Ohashi and Y. Terada, *Jpn. J. Appl. Phys.*, 1997, **36**, L289.
28 Z. Q. Chen, A. Kawasuso, Y. Xu, H. Naramoto, X. L. Yuan, T. Sekiguchi, R. Suzuki and T. Ohdaira, *Phys. Rev. B: Condens. Matter Mater. Phys.*, 2005, **71**, 115213.